JACS
JOURNAL OF THE AMERICAN CHEMICAL SOCIETY
Communication
pubs.acs.org/JACS

Self-Assembly of Molecule-like Nanoparticle Clusters Directed by DNA Nanocages

Yulin Li,[†] Zhiyu Liu,[†] Guimei Yu,[‡] Wen Jiang,[‡] and Chengde Mao*[,†]

[†]Department of Chemistry, Purdue University, West Lafayette, Indiana 47907, United States

[‡]Markey Center for Structural Biology and Department of Biological Sciences, Purdue University, West Lafayette, Indiana 47907, United States

Supporting Information

ABSTRACT: Analogous to the atom−molecule relationship, nanoparticle (NP) clusters (or NP-molecules) with defined compositions and directional bonds could potentially integrate the properties of the component individual NPs, leading to emergent properties. Despite extensive efforts in this direction, no general approach is available for assembly of such NP-molecules. Here we report a general method for building this type of structures by encapsulating NPs into self-assembled DNA polyhedral wireframe nanocages, which serve as guiding agents for further assembly. As a demonstration, a series of NP-molecules have been assembled and validated. Such NP-molecules will, we believe, pave a way to explore new nanomaterials with emergent functions/properties that are related to, but do not belong to the individual component nanoparticles.

Nanoparticles (NPs) have many interesting optical, electronic, and magnetic properties and have found a wide range of applications in catalysis, electronics, plasmonics, bioanalytics, etc.[1] Analogous to the atom−molecule relationship, NP clusters (or NP-molecules) with defined compositions and directional bonds could integrate the properties of the component NPs and, potentially, lead to emergent properties.[2] The properties of such NP-molecules depend on not only the chemical identities of the individual NPs but also the 3D organization of the NPs. Despite extensive efforts in this direction,[3] no general approach is available for assembly of NP-molecules in which NPs have defined valences and directional bonds. Here we report a general method for building such NP-molecules. Gold NPs (AuNPs) are encapsulated into self-assembled DNA polyhedral nanocages,[4] which serve as guiding agents for the further assembly of the AuNPs. To experimentally demonstrate this approach, a series of NP-molecules, including a one-core, five-NP, CH_4-like structure (with a tetrahedral symmetry); a one-core, seven-NP, SF_6-like structure (with an octahedral symmetry); a one-core, seven-NP, $W(CH_3)_6$-like structure (with a trigonal prismatic symmetry); and a two-core, eight-NP, C_2H_6-like structure (with a D_3 symmetry), have been assembled and validated by gel electrophoresis, transmission electron microscopy (TEM), and cryogenic electron microscopy (cryoEM).

Single-stranded DNA (ssDNA)-functionalized AuNPs (DNA-AuNPs) can assemble into large structures by DNA hybridization.[5−7] Multiple copies of ssDNAs are distributed around AuNPs similar to electrons in an s-orbital around an atom.[5,7] Such DNA-AuNPs are versatile building blocks and have been widely used in bioanalytics.[2] However, the high spherical symmetry of the ssDNA distribution limits the accessible structures of the AuNP assemblies. To achieve sophisticated architectures, it is essential to break the spherical symmetry.[2,3] In this work, we have explored using structural DNA nanotechnology[8−10] to overcome this problem. In recent years, a series of polyhedral-shaped DNA framework nanocages have been developed.[11] They can encapsulate DNA-AuNPs to form AuNP@DNA cage core−shell structures.[4] Confined in DNA polyhedra, the DNA-AuNPs lose their intrinsic spherical symmetry. Instead, the DNA polyhedral symmetries are imposed onto the DNA-AuNPs, giving the DNA-AuNPs defined valences and well-defined bonding directions (Figure 1). For example, being encapsulated into a DNA tetrahedron (TET), a DNA-AuNP can only interact with other DNA-AuNPs (via ssDNA hybridization) through the four faces of the TET because of both electrostatic repulsion and steric hindrance. Superficially, the ssDNAs on the AuNP in the

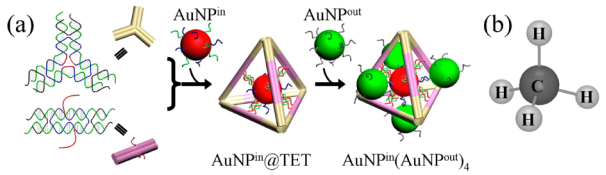

Figure 1. Self-assembly of methane-like NP-molecules. (a) In the assembly process, a DNA tetrahedron was assembled from DNA motifs (left; for details, see Supporting Information, Figures S1−S4). One gold NP ($AuNP^{in}$; red) was encapsulated into the DNA tetrahedron (TET) via DNA hybridization between the green strands on the $AuNP^{in}$ and the single-stranded tails on the TET. Incubated with the $AuNP^{in}$@TET core−shell complex, $AuNP^{out}$ will interact with the $AuNP^{in}$ via DNA hybridization between the gray single strands on the $AuNP^{out}$ and the blue strands on the $AuNP^{in}$. Due to both electrostatic effect and steric hindrance imposed by the TET, the $AuNP^{in}$ is accessible only from the four face centers of the TET. Thus, the $AuNP^{in}$ is tetravalent, and its four interacting bonds are defined by tetrahedral symmetry. The final complex has one $AuNP^{in}$ in the TET and four $AuNP^{out}$ outside of the TET. (b) For comparison, a methane molecule.

Received: February 3, 2015
Published: March 31, 2015

DOI: 10.1021/jacs.5b01196
J. Am. Chem. Soc. 2015, 137, 4320−4323

AuNP@TET complex resemble electrons in sp^3-orbitals of an atom instead of electrons in s-orbitals as for free DNA-AuNPs.

We first tested our strategy by assembly of tetrahedral NP-molecules that resemble the methane (CH_4) molecule (Figure 1). AuNPs (named $AuNP^{in}$; "in" stands for inside) were densely coated with multiple copies of two types of thiolated ssDNAs (colored green and blue, respectively). The green strands were complementary to and would hybridize with single-stranded tails (colored red) of a DNA TET, resulting in encapsulation of the $AuNP^{in}$ into the TET to form an $AuNP^{in}$@TET complex. Separately, another group of AuNP (named $AuNP^{out}$; "out" stands for outside) was coated with a third type of thiolated ssDNA (colored gray) with a sequence complementary to the blue strands immobilized on the $AuNP^{in}$. Upon mixing of the $AuNP^{out}$ and $AuNP^{in}$@TET complexes together, the gray DNA strands on $AuNP^{out}$ and the blue DNA strands on $AuNP^{in}$ would hybridize with each other and bring $AuNP^{out}$ and the $AuNP^{in}$@TET together to form large complexes. In the final complex, there was an $AuNP^{in}$ inside of the TET and an $AuNP^{out}$ at the outside center of each TET face. The overall structure $[AuNP^{in}(AuNP^{out})_4]$ resembles that of CH_4 with four hydrogen atoms in a tetrahedral arrangement around the center carbon atom.

$AuNP^{in\ 10}(AuNP^{out\ 10})_4$ (the superscript numbers indicate the NP diameters) is one of the CH_4-like NP-molecule. We monitored the assembly process with agarose gel electrophoresis (Figure 2a). Individual, free $AuNP^{in\ 10}$ had a high electrophoretic mobility. Upon mixed with the TET component DNA tiles and annealed, $AuNP^{in\ 10}$ was efficiently encapsulated into the TET to form $AuNP^{in\ 10}$@TET complexes. While the original $AuNP^{in\ 10}$ band completely disappeared, a new band with a lower mobility (corresponding to the $AuNP^{in\ 10}$@TET complex) appeared; suggesting the encapsulation was almost quantitative. After further incubation with excess amount of $AuNP^{out\ 10}$, the $AuNP^{in\ 10}$@TET band disappeared and a new band with an even slower mobility appeared, which corresponded to the $AuNP^{in\ 10}(AuNP^{out\ 10})_4$ molecule. The gel shift experiment suggested that the assembly process was very efficient. The composition of the NP-molecule was confirmed by TEM (Figure 2b). In the TEM image, individual NP-molecules were randomly distributed. In most of the NP-molecules, a 10 nm AuNP was surrounded by another four 10 nm AuNPs, consistent with the expected composition of the $AuNP^{in\ 10}(AuNP^{out\ 10})_4$ NP-molecule. In the CH_4-like NP-molecule, the sizes of both the inside and outside AuNPs can be varied. We tested this method with nine AuNP combinations (AuNP diameters of 5, 10, and 15 nm). All combinations resulted in desired structures (Figure 2c and Figures S5−13 in the Supporting Information). For different combinations, both assembly yield (73−98% as estimated by electrophoresis) and the purity (15−68% as evaluated by TEM) varied. In general, we observed high assembly yields and purities of the desired NP-molecules when small NPs were used. However, when large, 15 nm NPs were involved, the purities of the obtained NP-molecules decreased. Note that two different sized TETs were used to accommodate different-sized $AuNP^{in}$. For the small $AuNP^{in5}$, a small 4-turn TET (TET^{4t}) was used. Its struts were 4 helical turns (~14 nm) long. For the larger $AuNP^{in\ 10}$ and $AuNP^{in\ 15}$, a larger 8-turn TET (TET^{8t}) was used. Its struts were 8 helical turns (~28 nm) long.

To confirm that the assembled NP-molecules indeed had a tetrahedral structure, we imaged the $AuNP^{in\ 10}(AuNP^{out\ 10})_4$ molecule, one of the clusters, with cryoEM (Figures 3 and

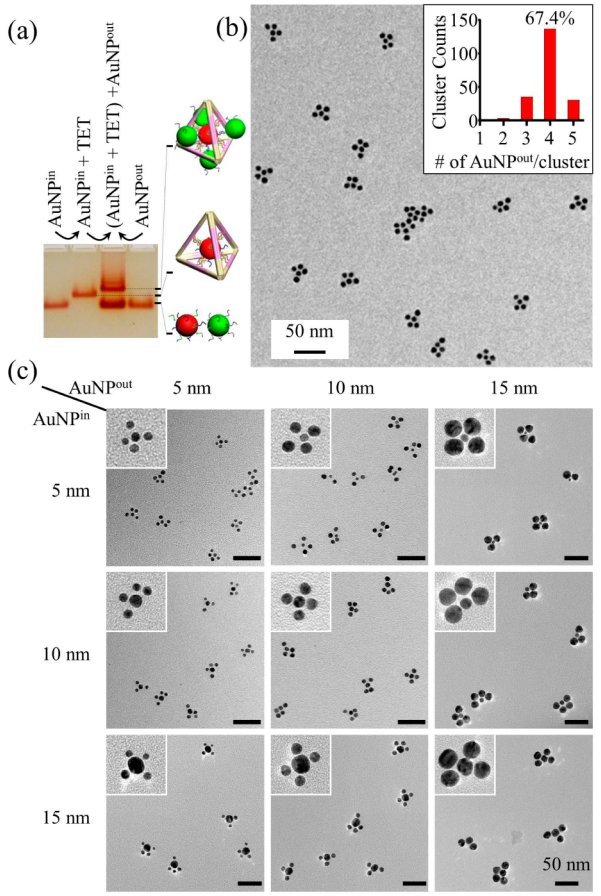

Figure 2. Characterization of methane (CH_4)-like NP-molecules. (a) Agarose gel monitoring the assembly process as exemplified by in the case of $AuNP^{in\ 10}(AuNP^{out\ 10})_4$ (superscript numbers indicate the AuNP diameters in nanometers). Sample compositions and band identities are indicated above and beside the gel, respectively. (b) A transmission electron micrograph (TEM) of $AuNP^{in\ 10}(AuNP^{out\ 10})_4$ shows that most of the NP clusters have four NPs around a central NP. Inset: Statistics of the $AuNP^{out}$ numbers in NP clusters observed in TEM imaging. (c) A graphic summary of $AuNP^{in}(AuNP^{out})_4$ with different NP diameters. Scale bars: 50 nm.

S14−S16), which would preserve the true 3D structures of the NP complex. The NP-molecules were randomly distributed in the raw image. While AuNPs had strong contrast and were easily observed, the DNA frames had too weak contrast to be observed. The AuNP clusters were randomly orientated during the cryoEM imaging (Figures 3a and S14). From the observed NP-molecules in cryoEM, we computationally reconstructed the original 3D architecture and obtained a CH_4-like tetrahedral configuration (Figure 3b). To verify the reconstructed architecture, we compared (i) the individual raw particles (Figure 3c) observed in cryoEM and (ii) the class average of the raw particles at similar orientations (Figure S16) with the computer-generated 2D projections of the reconstructed 3D model. Clearly, they matched with each other; thus confirming that the reconstructed model was indeed the native 3D configuration of the $AuNP^{in\ 10}(AuNP^{out\ 10})_4$ NP-molecule.

To demonstrate the generality of the assembly method, we further assembled another two NP complexes: a SF_6-like, octahedral NP-molecule and a $W(CH_3)_6$-like, triangular prismatic NP-molecule (Figure 4). Though having the same composition [containing a core NP ($AuNP^{in}$) and six peripheral

DOI: 10.1021/jacs.5b01196
J. Am. Chem. Soc. 2015, 137, 4320−4323

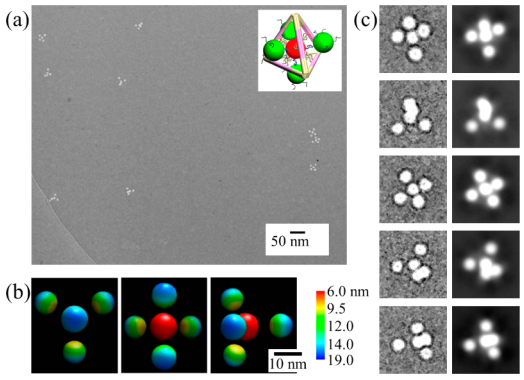

Figure 3. Study of CH_4-like $AuNP^{in\ 10}(AuNP^{out\ 10})_4$ NP-molecules by cryogenic electron microscopy (cryoEM). (a) A raw micrograph. The AuNPs appear as white spheres. Figure S14 presents a larger view of this image. (b) Three views of the 3D structural model reconstructed from the observed NP-molecules in cryoEM. The color indicates the distance from the center of the NP cluster. (c) Pairwise comparison between the raw cryoEM images (left) of individual $AuNP^{in\ 10}(AuNP^{out\ 10})_4$ NP-molecules and the 2D projections (right) back calculated from the reconstructed 3D model.

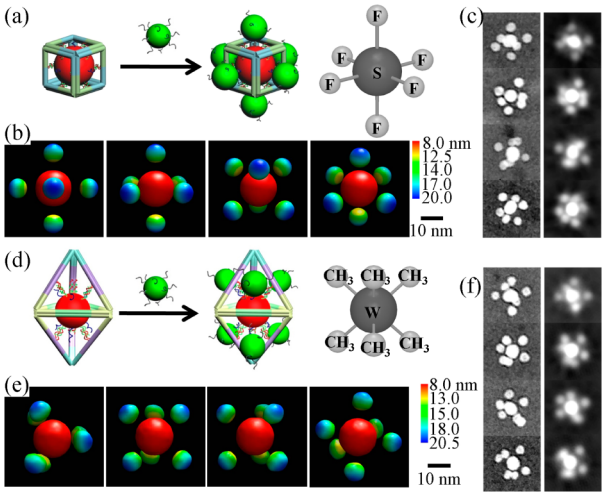

Figure 4. Self-assembly of octahedral SF_6-like and trigonal prismatic $W(CH_3)_6$-like NP-molecules guided by a DNA cube and a triangular bipyriamid (BiTET), respectively. Note that the two NP-molecules have the same composition $[AuNP^{in\ 15}(AuNP^{out\ 10})_6]$, but different configurations. (a,d) Assembly processes. On the right are the configurations of SF_6 and $W(CH_3)_6$. CryoEM characterization of (b,c) SF_6-like NP-molecule and (e,f) $W(CH_3)_6$-like NP-molecule. (b,e) Four views of the 3D structural models reconstructed from the observed NP-molecules in cryoEM imaging. The color indicates the distance from the center of the NP cluster. (c,f) Pairwise comparison between the raw cryoEM images (left) of individual NP-molecules and the 2D projections (right) back calculated from the reconstructed 3D models.

NPs (NPs^{out})], they have different symmetries and configurations. Thus, they are a pair of configuration isomers. To assemble these two NP complexes, we used two different types of DNA polyhedra as confining frameworks: a DNA cube and a triangular bipyramide (BiTET) for assembly of the octahedral and trigonal prismatic NP-molecule, respectively (Figure 4a,d). Both DNA polyhedra have six faces but with different 3D configurations. In each of the NP-molecule, six peripheral $AuNP^{out}$ bind to the encapsulated $AuNP^{in}$ near the face centers of the polyhedra. But the six $AuNP^{out}$ arranged differently in 3D space in the two complexes because of the different structures of the two DNA polyhedra. To confirm our hypothesis, we assembled those complexes with $AuNP^{in\ 15}$ and $AuNP^{out\ 10}$. As estimated by electrophoresis, the assembly yields were both ~90%. In TEM images, both assembled complexes show as clusters of an $AuNP^{in\ 15}$ surrounded by six $AuNP^{out\ 10}$ (Figures S17 and S18), indicating that the complex compositions $[AuNP^{in\ 15}(AuNP^{out\ 10})_6]$ were correct. The purities of the recovered samples were 38% and 43% for $(AuNP^{in}@Cube)$-$(AuNP^{out})_6$ and $(AuNP^{in}@BiTET)(AuNP^{out})_6$, respectively. However, there was no obvious difference between the two complexes because dehydration during TEM imaging caused the NP-molecules to collapse and lose their 3D structures. To reveal their native 3D structures, we applied cryoEM imaging to these NP-molecules (Figures 4b,c,e,f and S19–S24). From the raw images, we were able to reconstruct 3D models for the original NP-molecules. The reconstructed 3D models demonstrated clear differences between these two NP-molecules and were in good agreement with our design. The observed configuration difference between the pair of NP-molecule isomers strongly supported that guiding effect of the DNA polyhedra.

Our strategy was not limited to assembling NP-molecules with one core NP surrounded by several satellite NPs. We explored applying it to assemble more complex structures, such as a dual-core, ethane (C_2H_6)-like NP-molecule (Figures 5 and

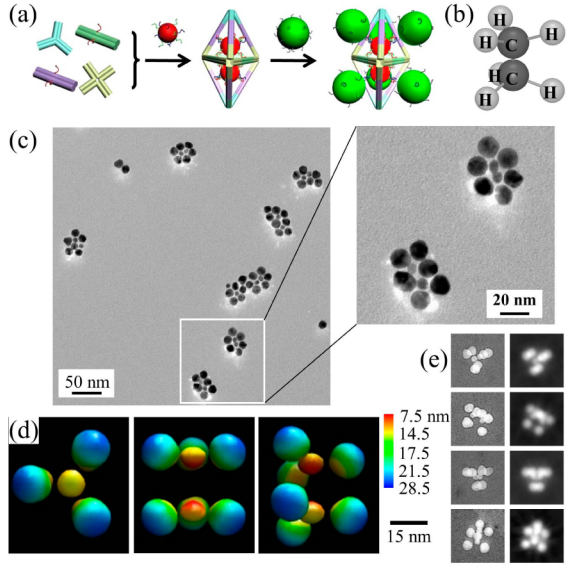

Figure 5. Self-assembly of a dual-core, ethane (C_2H_6)-like, NP-molecule guided by DNA BiTET. (a) The assembly scheme. (b) The C_2H_6 configuration. (c) A TEM image of the assembled C_2H_6-like NP-molecule and its close-up view. (d) Three views of the 3D structural model reconstructed from the observed NP-molecules in cryoEM imaging. The color indicates the distance from the NP cluster center. (e) Pairwise comparison between the raw cryoEM images (left) of individual NP-molecules and the 2D projections (right) back calculated from the reconstructed 3D models.

S25–S29). In this case, a DNA BiTET was used as the guiding polyhedron. As mentioned above, the 8-turn BiTET could encapsulate one 15 nm AuNP. However, when the smaller (10 nm) $AuNP^{10}$ was used, one BiTET could accommodate two $AuNP^{10}$ inside its cavity. In order to minimize the electrostatic repulsions and steric hindrance, the two $AuNP^{in\ 10}$ would be

DOI: 10.1021/jacs.5b01196
J. Am. Chem. Soc. 2015, 137, 4320–4323

separately located into the two tetrahedral chambers. The dual-encapsulation was efficient with a yield up to 70% (Figure S25). Due to the constraining effect of the DNA frameworks, each $AuNP^{in\ 10}$ would bind to three $AuNP^{out\ 15}$, which were located near the three face centers of its hosting TET chamber. The assembled NP-molecule $[(AuNP^{in\ 10})_2(AuNP^{out\ 15})_6]$ would resemble an ethane (C_2H_6) in terms of both composition and 3D figuration. After assembly (with 97% assembly yield), the sample was imaged by TEM (Figures 5c and S26). NP clusters were randomly distributed in the TEM field. In many (about 30%) of them, six large NPs surrounded two small NPs; confirming the designed composition. CryoEM study further confirmed the ethane-like configuration (Figures 5d,e and S27−S29).

In summary, we have developed a strategy to assemble molecule-like nanoparticle architectures with specific 3D directional bonding. In the NP-molecules, multiple interactions (DNA hybridizations) exist between any two interacting NPs and greatly reduce structural flexibility. Due to the availability of various DNA polyhedral nanocages,[11] a rich variety of NP-molecules should be accessible. The NP sizes can be adjusted as demonstrated in this work. It is also possible to expand the chemical identities of the NPs to other materials, such as quantum dots and magnetic nanoparticles,[12] as long as they can be functionalized with oligonucleotides. We expect the construction of such NP-molecules will pave a way to explore new nanomaterials with functions/properties that are related to, but do not belong to the individual component nanoparticles.[2]

■ ASSOCIATED CONTENT

Supporting Information

Materials, methods, and additional experimental data. This material is available free of charge via the Internet at http://pubs.acs.org.

■ AUTHOR INFORMATION

Corresponding Author

*mao@purdue.edu

Notes

The authors declare no competing financial interest.

■ ACKNOWLEDGMENTS

We thank the National Science Foundation for support.

■ REFERENCES

(1) (a) Daniel, M.-C.; Astruc, D. *Chem. Rev.* **2004**, *104*, 293−346. (b) Nie, Z.; Petukhova, A.; Kumacheva, E. *Nat. Nanotechnol.* **2010**, *5*, 15−25. (c) Giljohann, D. A.; Seferos, D. S.; Daniel, W. L.; Massich, M. D.; Patel, P. C.; Mirkin, C. A. *Angew. Chem., Int. Ed.* **2010**, *49*, 3280−3294.

(2) (a) Kuzyk, A.; Schreiber, R.; Fan, Z.; Pardatscher, G.; Roller, E.-M.; Hogele, A.; Simmel, F. C.; Govorov, A. O.; Liedl, T. *Nature* **2012**, *483*, 311−314. (b) Tikhomirov, G.; Hoogland, S.; Lee, P. E.; Fischer, A.; Sargent, E. H.; Kelley, S. O. *Nat. Nanotechnol.* **2011**, *6*, 485−490. (c) Schreiber, R.; Do, J.; Roller, E.-M.; Zhang, T.; Schuller, V. J.; Nickels, P. C.; Feldmannn, J.; Liedl, T. *Nat. Nanotechnol.* **2014**, *9*, 74−78. (d) Liu, J.; Lu, Y. *J. Am. Chem. Soc.* **2003**, *125*, 6642−6643. (e) Sonnichsen, C.; Reinhard, B. M.; Liphardt, J.; Alivisatos, A. P. *Nat. Biotechnol.* **2005**, *23*, 741−745. (f) Lan, X.; Chen, Z.; Dai, G.; Lu, X.; Ni, W.; Wang, Q. *J. Am. Chem. Soc.* **2013**, *135*, 11441−11444. (g) Shen, X.; Song, C.; Wang, J.; Shi, D.; Wang, Z.; Liu, N.; Ding, B. *J. Am. Chem. Soc.* **2012**, *134*, 146−149. (h) Kuzyk, A.; Schreiber, R.; Zhang, H.; Govorov, A. O.; Liedl, T.; Liu, N. *Nat. Mater.* **2014**, *13*, 862−866.

(3) (a) Mastroianni, A. J.; Claridge, S. A.; Alivisatos, A. P. *J. Am. Chem. Soc.* **2009**, *131*, 8455−8459. (b) Li, Y.; Zheng, Y.; Gong, M.; Deng, Z. *Chem. Commun.* **2012**, *48*, 3727−3729. (c) Tan, L. H.; Xing, H.; Chen, H.; Lu, Y. *J. Am. Chem. Soc.* **2013**, *135*, 17675−17678. (d) Sharma, J.; Chhabra, R.; Cheng, A.; Brownell, J.; Liu, Y.; Yan, H. *Science* **2009**, *323*, 112−116. (e) Wang, Y.; Wang, Y.; Breed, D. R.; Manoharan, V. M.; Feng, L.; Hollingsworth, A. D.; Weck, M.; Pine, D. J. *Nature* **2012**, *491*, 51−55. (f) Jones, M. R.; Mirkin, C. A. *Nature* **2012**, *491*, 42−43. (g) Chen, Q.; Bae, S. C.; Granick, S. *J. Am. Chem. Soc.* **2012**, *134*, 11080−11083. (h) DeVries, G. A.; Brunnbauer, M.; Hu, Y.; Jackson, A. M.; Long, B.; Neltner, B. T.; Uzun, O.; Wunsch, B. H.; Stellacci, F. *Science* **2007**, *315*, 358−361. (i) Jones, M. R.; Macfarlane, R. J.; Lee, B.; Zhang, J.; Young, K. L.; Senesi, A. J.; Mirkin, C. A. *Nat. Mater.* **2010**, *9*, 913−917. (j) Zhao, Z.; Jacovetty, E. L.; Liu, Y.; Yan, H. *Angew. Chem., Int. Ed.* **2011**, *50*, 2041−2044. (k) Sun, W.; Boulais, E.; Hakobyan, Y.; Wang, W. L.; Guan, A.; Bathe, M.; Yin, P. *Science* **2014**, *346*, 1258361.

(4) Zhang, C.; Li, X.; Tian, C.; Yu, G.; Li, Y.; Jiang, W.; Mao, C. *ACS Nano* **2014**, *8*, 1130−1135.

(5) Mirkin, C. A.; Letsinger, R. L.; Mucic, R. C.; Storhoff, J. J. *Nature* **1996**, *382*, 607−609.

(6) Alivisatos, A. P.; Johnsson, K. P.; Peng, X.; Wilson, T. E.; Loweth, C. J.; Bruchez, M. P., Jr; Schultz, P. G. *Nature* **1996**, *382*, 609−611.

(7) (a) Nykypanchuk, D.; Maye, M. M.; van der LeLie, D.; Gang, O. *Nature* **2008**, *451*, 549−552. (b) Park, S. Y.; Lytton-Jean, A. K. R.; Lee, B.; Weigand, S.; Schatz, G. C.; Mirkin, C. A. *Nature* **2008**, *451*, 553−556.

(8) Jones, M. R.; Seeman, N. C.; Mirkin, C. A. *Science* **2015**, *347*, No. 1260901.

(9) Seeman, N. C. *Nature* **2003**, *421*, 427−431.

(10) Zhang, F.; Nangreave, J.; Liu, Y.; Yan, H. *J. Am. Chem. Soc.* **2014**, *136*, 11198−11211.

(11) (a) Shih, W. M.; Quispe, J. D.; Joyce, G. F. *Nature* **2004**, *427*, 618−621. (b) Goodman, R. P.; Schaap, I. A. T.; Tardin, C. F.; Erben, C. M.; Berry, R. M.; Schmidt, C. F.; Turberfield, A. J. *Science* **2005**, *310*, 1661−1665. (c) He, Y.; Ye, T.; Su, M.; Zhang, C.; Ribbe, A. E.; Jiang, W.; Mao, C. *Nature* **2008**, *452*, 198−201. (d) Zhang, C.; Ko, S. H.; Su, M.; Leng, Y.; Ribbe, A. E.; Jiang, W.; Mao, C. *J. Am. Chem. Soc.* **2009**, *131*, 1413−1415. (e) Tian, C.; Li, X.; Liu, Z.; Jiang, W.; Wang, G.; Mao, C. *Angew. Chem., Int. Ed.* **2014**, *53*, 8041−8044. (f) Linuma, R.; Ke, Y.; Jungmann, R.; Schlichthaerle, T.; Woehrstein, J. B.; Yin, P. *Science* **2014**, *344*, 65−69.

(12) Zhang, C.; Marfarlane, R. J.; Young, K. L.; Choi, C. H. J.; Hao, L.; Auyeung, E.; Liu, G.; Zhou, X.; Mirkin, C. A. *Nat. Mater.* **2013**, *12*, 741−746.

DOI: 10.1021/jacs.5b01196
J. Am. Chem. Soc. 2015, 137, 4320−4323